REFERENCES AND NOTES

1. B. Haq, J. Hardenbol, P. Vail, *Science* **23**, 1156 (1987).
2. S. O. Schlanger, in *Mesozoic and Cenozoic Oceans*, K. Hsu, Ed. (American Geophysical Union, Washington DC, 1986), pp. 61–74.
3. A. Hallam, *Phanerozoic Sea-Level Changes* (Columbia Univ. Press, New York, 1992).
4. K. K. Turekian and J. L. Kulp, *Geochim. Cosmochim. Acta* **10**, 245 (1956).
5. S. O. Schlanger, in *Physical and Chemical Weathering in Geochemical Cycles*, A. Lerman and M. Meybeck, Eds. (Kluwer, Boston, MA, 1988), pp. 323–340.
6. E. Gavish and G. Friedman, *J. Sediment. Petrol.* **39**, 980 (1969); W. H. Harris and R. K. Matthews, *Science* **160**, 77 (1968).
7. B. N. Opdyke and B. H. Wilkinson, *Paleoceanography* **3**, 685 (1988).
8. Sites 391C and 534A are located in the Blake-Bahama Basin off the coast of Florida, and site 603B is located approximately 1000 km to the northeast, off the coast of Virginia.
9. Stable isotope measurements of bulk carbonate were made on a VG Optima gas-source mass spectrometer at Princeton University. Precision (1σ) is 0.05 per mil for $\delta^{18}O$ and 0.03 per mil for $\delta^{13}C$.
10. T. J. Bralower, S. Moneci, H. R. Thierstein, *Mar. Micropaleontol.* **14**, 153 (1989).
11. Sr was measured in bulk carbonate and normalized to 100% $CaCO_3$, measured as acid-insoluble residue or by Ca content. Sr and Ca determinations were made in 1.0 N acetic acid dissolutions by atomic adsorption spectroscopy. Reproducibility is better than 1% (coefficient of variation).
12. H. M. Stoll and D. P. Schrag, data not shown.
13. M. R. Palmer and J. M. Edmond, *Earth Planet. Sci. Lett.* **92**, 11 (1989).
14. The smoothed records reduce the maximum amplitude of the Sr increases from 120 to 80%.
15. Bulk carbonate was flushed with 1.0 N ammonium acetate to remove Sr adsorbed on exchange sites. The carbonate residue was then dissolved in 1.0 N acetic acid as in (*13*).
16. P. Baker, J. M. Gieskes, H. Elderfield, *J. Sediment. Petrol.* **52**, 52 (1982); F. M. Richter and D. J. DePaolo, *Earth Planet. Sci. Lett.* **83**, 27 (1987).
17. F. M. Richter and Y. Liang, *Earth Planet. Sci. Lett.* **117**, 553 (1993).
18. A third-order polynomial fit to long-term variations in $\delta^{18}O$ in each record was subtracted from $\delta^{18}O$. These detrended oxygen isotope data are expressed as per mil increases over the minimum value.
19. N. J. Shackleton, M. A. Hall, D. Pate, *Paleoceanography* **8**, 141 (1993).
20. D. P. Schrag, D. J. DePaolo, F. M. Richter, *Geochim. Cosmochim. Acta* **59**, 2265 (1995).
21. D. P. Schrag, D. J. DePaolo, F. M. Richter, *Earth Planet. Sci. Lett.* **111**, 305 (1992).
22. The effect of Ca variability on Sr partitioning is not included in the model, because the riverine-hydrothermal flux is held constant and Ca is not released during aragonite recrystallization. Initial Sr model concentrations are 1650 ppm for aragonite and 500 ppm for calcite.
23. D. Archer and E. Maier-Reimer, *Nature* **367**, 260 (1994); B. N. Opdyke and J. C. G. Walker, *Geology* **20**, 733 (1992).
24. R. K. Matthews and C. Frohlich, *Geology* **15**, 673 (1987). A smaller amount of total recrystallization scales with the total amount of sea level change implied by the model.
25. We obtained the composite sea level curve by averaging all three $\delta^{18}O$ records, inverting the result, and normalizing to a specified magnitude of sea level change.
26. E. J. Barron, W. W. Hay, E. G. Kauffman, *Geology* **12**, 377 (1984); E. J. Barron, *ibid.*, p. 595.
27. L. A. Frakes, J. E. Francis, J. I. Syktus, *Climate Modes of the Phanerozoic* (Cambridge Univ. Press, New York, 1992).
28. M. L. Prentice and R. K. Matthews, *J. Geophys. Res.* **96**, 6811 (1991).
29. L. A. Frakes and J. E. Francis, *Nature* **333**, 547 (1988).
30. R. K. Matthews and C. Frohlich, *J. Geophys. Res.* **96**, 6797 (1991).

31. Supported in part by an Office of Naval Research graduate fellowship to H.M.S. Conversations with F. Richter, M. Monahan, and P. Koch were instrumental in developing this project.

6 February 1996; accepted 19 April 1996

Fine-Scale Doppler Radar Observations of Tornadoes

Joshua Wurman,* Jerry M. Straka,* Erik N. Rasmussen

Observations obtained with a mobile pencil-beam Doppler radar revealed many previously unresolved structures within tornadic storms and tornadoes and helped verify various aspects of conceptual models. Radar data from the parent circulations indicate the existence of spiral reflectivity bands, intense radial wind shear zones, and multiple larger-scale velocity maxima. Tornado structures observed include debris shields, clear axial (eye) regions, multiple reflectivity bands surrounding the center of the eye, and occasional reflectivity protrusions into the eye. Velocity and reflectivity data from tornado-scale circulations show evidence of axial downdrafts.

A widely accepted conceptual model of the flow regions in and around a tornado (Fig. 1) has been developed over the past two decades on the basis of numerous theoretical, numerical, and observational studies (*1*–*6*). The vortex of the tornado is embedded in a swirling, rising outer-flow region (region I), which usually is associated with the parent thunderstorm mesocyclone on a larger scale (radius 5 to 10 km) and with the tornado cyclone on a somewhat smaller scale (radius 1 to 3 km). The flow approximately conserves angular momentum in this region. The core region of the tornado (region II) is thought to be nearly axisymmetric and is characterized by flow that spirals radially inward and upward. This region extends out to about the radius of the maximum tangential winds. The winds in this regime are approximately in cyclostrophic balance (a balance between the horizontal pressure gradient force and the centrifugal force), which helps suppress turbulence and radial flow. Cyclostrophic pressure deficits associated with stronger rotation in the lower levels than in the upper levels can accelerate the movement of air downward along the central axis. The corner-flow region in the tornado (region III) is characterized by intense, frictionally induced, radial inflow that must turn abruptly upward, owing to vertical pressure gradients, before reaching the axis. In the surface boundary layer region (region IV), friction produced by the lower boundary (the Earth's surface) retards the rotating flow. This disrupts the cyclostrophic wind balance, and flow accelerates radially inward toward the axis of rotation. Finally, the convective plume region (region V) is where angular momentum concentrated in the lower levels of the tornado circulation is transported outward by divergence or turbulence. Up to this time, observations to verify this conceptual model of a tornado have been unavailable.

In this report, we present close-range (2 to 6 km), fine-scale resolution volume (50 to 130 m), 3-cm band radar reflectivity and pulsed Doppler weather radar observations of a violent tornado that were obtained as part of the Verification of the Origins of Rotation in Tornadoes Experiment (VORTEX) field program (*7*). Earlier pulsed Doppler radar observations of tornadoes have been at more distant ranges (12 to 60 km), resulting in wider resolution volume

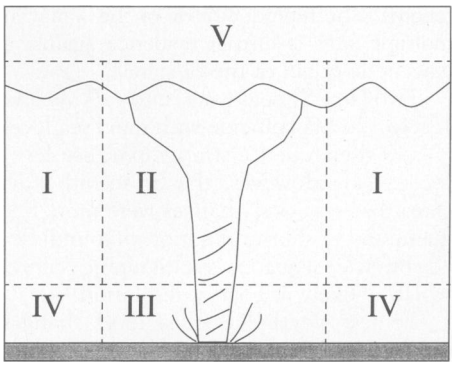

Fig. 1. Conceptual model of the flow regimes associated with a tornado: region I, outer flow; region II, core; region III, corner; region IV, surface boundary layer; region V, convective plume (*1*–*6*).

J. Wurman, School of Meteorology, University of Oklahoma, 100 East Boyd Street, Norman, OK 73019, USA.
J. M. Straka, School of Meteorology, Center for Analysis and Prediction of Storms and Cooperative Institute for Mesoscale Meteorological Studies, University of Oklahoma, 100 East Boyd Street, Norman, OK 73019, USA.
E. N. Rasmussen, National Severe Storms Laboratory, 1313 Halley Circle, Norman, OK 73069, USA.

*These authors contributed equally to this work.

widths (200 to 1000 m) that are too large to resolve detailed structures (8). Wide-beam, continuous-wave Doppler measurements of tornadoes have been made at ranges of 2 to 5 km, but these have only provided information about velocity maxima and spectra (8, 9). The high-resolution radar reflectivity and Doppler data presented herein provide four-dimensional reflectivity and velocity information that are essential to evaluate conceptual models of tornadic storms and tornadoes.

We obtained data with a mobile pulsed Doppler weather radar, the Doppler on Wheels (DOW) (*10, 11*) (Fig. 2). The radar was mounted on a small truck and radiated through a scanning 1.83-m parabolic dish, resulting in a 1.2° beam. The transmitter operated at 9.375 GHz (32 mm), sending 40-kW pulses with a duration of 450 ns every 500 μs. Meteorological signals as weak as −25 dB of equivalent radar reflectivity factor (dBZ) could be detected at ranges <3 km. The deployment time for the radar was 60 to 120 s.

At about 00:58 UTC (universal time coordinated) on 3 June 1995, a violent tornado formed to the south of Dimmitt, Texas, and traveled toward the northeast and north at speeds of 5 to 15 m s^{-1}. The tornado destroyed a home, lofted automobiles, and removed asphalt from a region of highway 10 m by 40 m and deposited it up to 200 m away. We used the mobile radar to observe the tornado in its intense mature stage from 5 min after formation until it dissipated 14 min later. The axis of the tornado approached within 3 km of the radar and remained within 4 km for 10 min. Data were collected in eight scans through the lower 1 to 2 km (depending on range) of the atmosphere with volume update intervals of 95 s (*12*). Oversampling of the data provided azimuthal samples every 17 m at a range of 3 km.

Numerous fine-scale tornado structures were revealed in the reflectivity and velocity fields. A prominent feature at 01:03:45 UTC at 110 m above ground level (AGL) was a 200-m-wide weak reflectivity region, referred to as the eye, in the center of the tornadic circulation (Fig. 3A). Surrounding the eye was a ring or band of large reflectivity 700 m in diameter and 200 to 300 m wide. The diameter of the reflectivity ring was consistent with the size of the debris shield produced by the tornado at this time, as estimated from photogrammetry and a damage survey. Small-scale structures 100 to 150 m in diameter in the reflectivity ring probably were irregularities in the debris shield.

About 3 to 4 min later, at 01:07:20 UTC, other structures were observed in the tornado, including multiple, semiconcentric to concentric, rings or bands of reflectivity surrounding the center of the eye (Fig. 4) and occasional reflectivity protrusions in the eye. At 6° elevation, the inner reflectivity band was 400 m in diameter and the outer band was 1100 m in diameter. Both bands were complete and nearly circular at this elevation; the inner one surrounded the eye region. At 14° elevation, the inner band was not complete. However, a reflectivity protrusion in the eye region was evident on the east-northeast side of the tornado in association with the inner reflectivity band. A tentative explanation for the multiple bands includes sorting of particles with various characteristic masses (for example, raindrops versus debris). It is likely, on the basis of photogrammetry, that the inner reflectivity band was associated with the visual tornado, at least at this time, whereas the outer band was associated with the lofting of large amounts of debris on only one side of the tornado or with inhomogeneous sources of

Fig. 2. DOW mobile radar with Dimmitt, Texas, tornado in background. The range to the edge of the cone-shaped visible debris shield around the tornado is approximately 2.5 km.

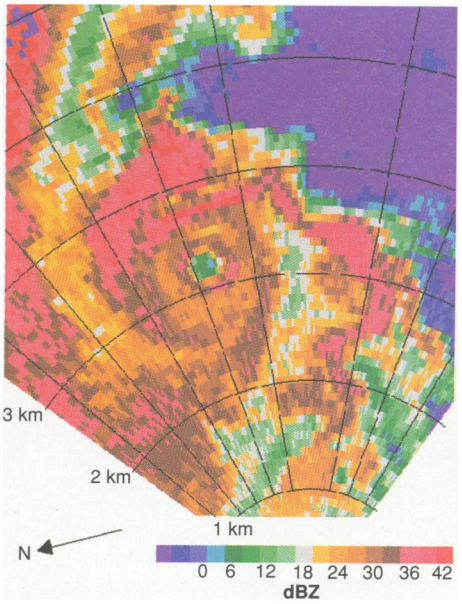

Fig. 4. Radar reflectivity field of the tornado and near-tornado environment in Dimmitt, Texas, at 01:07:20 UTC on 3 June 1995 as measured by DOW from a range of 3 km (*12*). These data were taken with a scan at 6° elevation or about 330 m AGL at the center of the tornado. Each displayed sample is approximately 64 m by 17 m at the center of the tornado. Two concentric bands of enhanced radar reflectivity surround the axial region of the tornado.

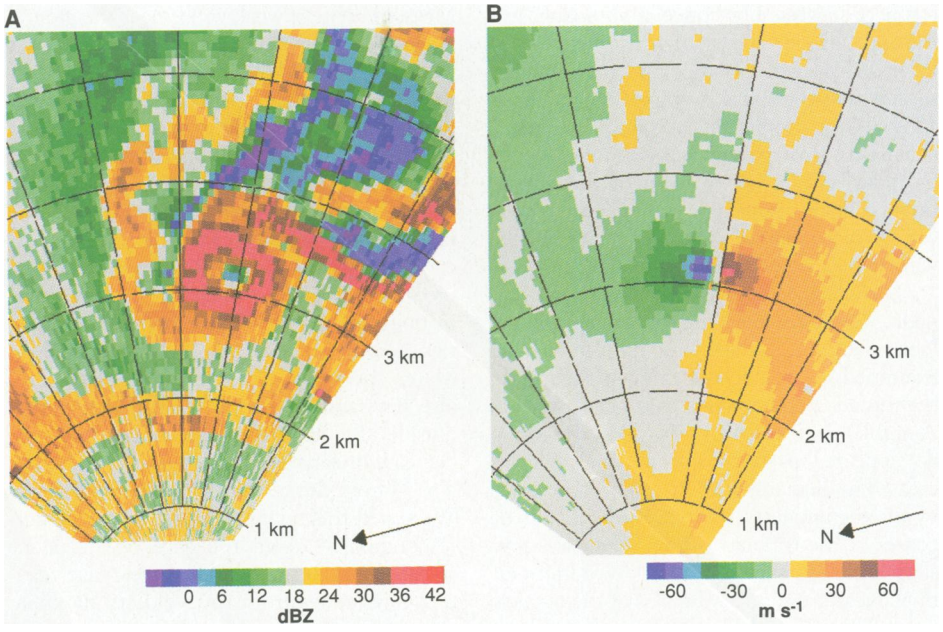

Fig. 3. Radar reflectivity and Doppler velocity fields of the tornado and near-tornado environment in Dimmitt, Texas, at 01:03:45 UTC on 3 June 1995 as measured by DOW from a range of 3 km (*12*). These data were taken with a scan at 2° elevation or 110 m AGL at the center of the tornado. Each displayed sample is approximately 64 m by 17 m at the center of the tornado. (**A**) Radar reflectivity. A small eye, free of substantial amounts of debris and rain, is surrounded by a nearly circular wall of debris. (**B**) Doppler radial velocities (velocities along a radar beam): Cyclonic shear (anticlockwise) is indicated by adjacent velocities that are away (positive) and toward (negative) radar. A strong cyclonic shear region is present in the tornado. Maximum winds are estimated to be >70 m s^{-1}.

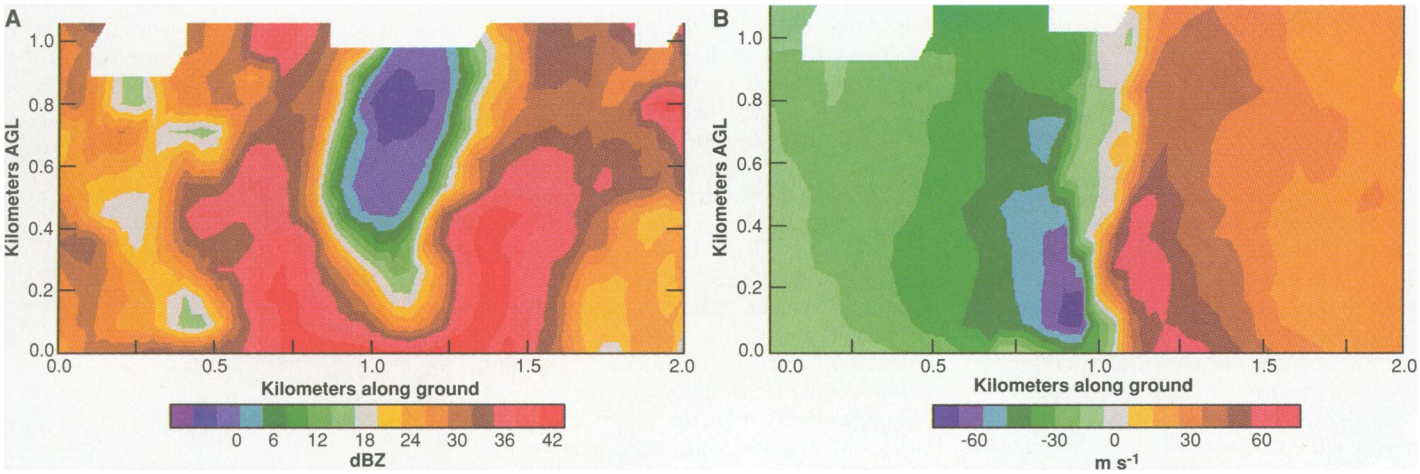

Fig. 5. Vertical structure of reflectivity and Doppler velocity fields of tornado and near-tornado environment at 01:03:26 to 01:05:01 UTC on 3 June 1995 as measured by DOW from a range of 3 km. These fields were reconstructed from 10 inclined slices (*12*) through the storm that were measured during a 95-s period. (**A**) Radar reflectivity. A deep eye with weak reflectivity penetrated through the depth of the cross section and was surrounded by a debris shield that extended from the surface to above 800 m AGL. (**B**) Doppler radial velocity. Strong tangential flow near the tornado core peaked at >70 m s^{-1} at 100 m AGL. The relatively broad region of 6 to 9 m s^{-1} toward the radar in the eye above 500 m AGL provides evidence of downward motion.

debris, or possibly with debris lofted by intense vertical motions in a suction vortex.

Doppler radial velocities at ~110 m AGL (Fig. 3B) revealed a strong shear couplet associated with the tornado (*2*, *13*, *14*). Maximum velocities on the north and south sides of the tornado circulation were >70 m s^{-1} (*15*, *16*), resulting in a velocity difference of approximately 140 m s^{-1} at a radius of 60 to 100 m. The vertical component of shear vorticity in the tornado was 0.7 to 1.1 s^{-1}. Unexpectedly, strong radial convergence into the tornado, suggested by conceptual models, was not indicated by the radar at the very lowest levels. However, photogrammetric analyses suggest that there was strong inflow in a layer 10 to 20 m deep near the ground. Convergence and stronger winds were not observed by radar within 20 to 30 m of the ground because radar beams may have been too wide (60 m at a range of 3 km) or contaminated with signals from ground clutter.

To further examine structures in the tornado, we interpolated the reflectivity and velocity data onto a Cartesian grid (*16*, *17*) and examined a vertical slice through the axis of the tornado perpendicular to the radar (Fig. 5, A and B). In the reflectivity fields, the tornado appeared as a truncated cone that increased in diameter with height, as confirmed by photogrammetry. A backward shift of the center of the tornado below 200 m was possibly caused by surface drag or downdraft outflow. Near the surface, the axis of the tornado was filled with debris, which produced large reflectivities. Above the surface, the eye region widened from 200 m at 75 m AGL to 400 m at 1000 m AGL. Owing to centrifugal effects, the debris lofted by the tornado was displaced outward and produced a ring of debris and large reflectivities surrounding the eye. The outer edge of the large reflectivity values produced by the debris was approximately coincident with the region where winds were near 30 m s^{-1}. The largest reflectivity maxima associated with the shield were noticeable to heights of over 800 m AGL.

The strongest tangential winds in the tornado ranged from >70 m s^{-1} below 200 m AGL to 50 to 70 m s^{-1} above 600 m AGL (Fig. 5B). These winds were found on the inside perimeter of the debris shield at a radius of about 60 to 100 m in the lower levels of the tornado and 200 to 300 m in the upper levels. Measurements of weak winds near the ground (<50 m AGL) are probably erroneous, as discussed above. These observations support theories (*1*–*6*) that the height of the maximum tangential winds in a tornado should occur within 100 to 200 m AGL, below the top of the tornado's boundary layer. Maximum wind speeds are believed to exceed those predicted by pure cyclostrophic balance because air parcels in the boundary layer approach closer to the axis than those above and in doing so acquire higher tangential velocities despite some angular momentum loss. Many theoretical and laboratory estimates also have indicated that tangential speeds V outside the maximum speed region should decrease linearly with the inverse of radius ($V \propto r^{-1}$) from the center of the rotation (*1*–*6*). We tested this relation out to a distance corresponding to about the edge of the debris cloud. Starting at two or more radar resolution volumes from the velocity maxima, the correlation for this relation was >0.85 in the lower levels of the tornado, and >0.95 in the higher levels. The poorer correlation fit in the lower levels may have been related to the presence of unresolved subvortex scale structures in the data.

The radar reflectivity and velocity fields show that there may have been a downdraft in the axial region of the vortex. Whether downdrafts occur in tornadoes has been controversial (*1*–*6*). The weak reflectivity region in the eye, which appeared abruptly above the surface, could be explained by axial downdrafts in the core, which would have prevented debris from rising in the core of the tornado. A weak reflectivity eye might also form as a result of centrifuging effects arising from strong tangential flow. However, the presence of a downdraft of >25 m s^{-1} in the eye region was indicated by persistent radial flow of 6 to 9 m s^{-1} toward the radar between 400 to 1000 m AGL along the tornado axis (Fig. 5B). This estimate of downward motion was inferred from the relation $W = V_r/\sin\Theta$, where W is the vertical motion, V_r is the measured radial velocity, and Θ is the elevation angle of the radar. In this calculation, it was assumed that the scattering phenomenon, either Bragg scattering (*14*) or scattering by uncentrifuged particles, was moving at the wind velocity. During much of the observation period, the tornado moved along a path tangent to the radar beams; thus, velocity data did not include any significant component of the tornado translation.

REFERENCES AND NOTES

1. W. S. Lewellen, in *Proceedings, Symposium on Tornadoes: Assessment of Knowledge and Implications for Man* (Texas Tech University, Lubbock, 1976), pp. 107–143.
2. C. D. Church, J. T. Snow, E. M. Agee, *Bull. Am. Meteorol. Soc.* **58**, 900 (1977).
3. R. P. Davies-Jones, in *Thunderstorm Morphology and Dynamics*, E. Kessler, Ed. (Univ. of Oklahoma Press, Norman, OK, ed. 2, 1986), pp. 197–236.
4. R. Rotunno, in *Mesoscale Meteorology and Forecasting*, P. S. Ray, Ed. (American Meteorological Society, Boston, MA, 1986), pp. 414–436.
5. W. S. Lewellen, in *The Tornado: Its Structure, Dynamics, Prediction, and Hazards* (*Geophys. Monogr. Am. Geophys. Union* **79**, American Geophysical Union, Washington, DC, 1993), pp. 19–39.

6. J. T. Snow, *Rev. Geophys Space Phys.* **20**, 953 (1982).
7. E. A. Rasmussen *et al.*, *Bull. Am. Meteorol. Soc.* **75** 995 (1994).
8. H. B. Bluestein and J. H. Golden, in *The Tornado: Its Structure, Dynamics, Prediction and Hazards* (*Geophys. Monogr. Am. Geophys. Union* **79**, American Geophysical Union, Washington, DC, 1993), pp. 319–352.
9. H. B. Bluestein, J. G. LaDue, H. Stein, D. Speeder, W. P. Unruh, *Mon. Weather Rev.* **121**, 2200 (1993).
10. J. Wurman, J. M. Straka, E. N. Rasmussen, M. Randall, A. Zahrai, preprint, 27th American Meteorlogical Society International Conference on Radar Meteorology, Aspen, CO, 1995.
11. ———, in preparation.
12. We made scans at elevation angles of 0°, 1°, 2°, 4°, 6°, 8°, 10°, 12°, 14°, and 18° elevation, every 95 s, with a scan rate of 10° s^{-1}, using 64 pulses per beam and a Nyquist interval of 32 m s^{-1}. Plotted radar times were 2 min ahead of UTC.
13. The Doppler velocity data contained folds at ±16 and ±48 m s^{-1}, which were manually unfolded to produce the velocity fields shown in the figures.
14. R. J. Doviak and D. S. Zrnic', *Doppler Radar and Weather Observations* (Academic Press, New York, 1993).
15. Small-scale suction vortices, 10 to 30 m in diameter, were not unambiguously revealed in either the 50- to 75-m radar resolution volumes of reflectivity or in velocity data retrieved at Dimmitt, TX. It is possible that higher velocities exist in these features, although this was not indicated by the damage survey. Very few structures were struck and therefore damaged by this tornado.
16. We used the following software packages to analyze the data and produce the figures: Solo (to display and unfold raw data); Reorder (to interpolate to Cartesian grids); and Zebra (to display gridded data), developed by the Research Data Program of the Atmospheric Technology Division at the National Center for Atmospheric Research (NCAR).
17. An advective correction of 6.2 m s^{-1} from 185° (from just west of south) was applied to correct for the time skew between low- and high-altitude observations. The grid spacing was 50 m. The nearest-neighbor method was used to interpolate to the Cartesian grid.
18. Supported by the University of Oklahoma (J.M.S. and J.W.); the National Oceanic and Atmospheric Administration, National Severe Storms Laboratory (NSSL) (E.N.R., J.M.S., and J.W.); NCAR, Atmospheric Technology Division, Remote Sensing Facility (J.W.); and the Center for the Analysis and Prediction of Storms through NSF grant ATM-912 0009 (J.M.S. and J.W.). The Cooperative Institute for Mesoscale Meteorological Studies, at the University of Oklahoma, also played an important role. The truck for the mobile radar was provided by NSSL (R. Maddox and D. Forsythe), and the radar transmitter was provided by NCAR (D. Carlson and P. Hildebrand). M. Randall and E. Loew provided the software and hardware for the PC Integrated Radar Acquisition data acquisition system. A. Zahari designed the antenna controller. D. Nealson and P. Griffin provided assistance in building and maintaining the radar. L. Chan prepared this manuscript.

12 February 1996; accepted 3 May 1996

Ion-Induced Morphological Changes in "Crew-Cut" Aggregates of Amphiphilic Block Copolymers

Lifeng Zhang, Kui Yu, Adi Eisenberg*

The addition of ions in micromolar ($CaCl_2$ or HCl) or millimolar (NaCl) concentrations can change the morphology of "crew-cut" aggregates of amphiphilic block copolymers in dilute solutions. In addition to spherical, rodlike, and univesicular or lamellar aggregates, an unusual large compound vesicle morphology can be obtained from a single block copolymer. Some features of the spontaneously formed large compound vesicles may make them especially useful as vehicles for delivering drugs and as models of biological cells. Gelation of a dilute spherical micelle solution can also be induced by ions as the result of the formation of a cross-linked "pearl necklace" morphology.

Most aggregates formed by the self-assembly of amphiphilic block copolymers in selective solvents are spherical and consist of a core and a coronal shell. The core is composed of the insoluble blocks, whereas the corona contains the soluble blocks, which are highly swollen by the solvent. Such structures have been explored in detail (*1*). We have described the formation of aggregates of multiple morphologies of one family of highly asymmetric polystyrene-*b*-poly(acrylic acid) (PS-*b*-PAA) in dilute solution (*2*) in which the length of the insoluble PS blocks was much longer than that of the soluble PAA blocks. They were therefore described as "crew-cut" aggregates. As the length of the PAA block decreased, the morphology of the aggregate changed from spherical to rodlike, to lamellar or vesicular, and finally to large compound micelles (LCMs) consisting of an assembly of inverted spherical micelles surrounded by a hydrophilic surface. A more detailed description of the multiple morphologies and the characteristics of the crew-cut micellelike aggregates is available (*3*). More recently, it was shown that PS-*b*-poly(ethylene oxide) (PS-*b*-PEO) diblocks in dilute solution can also form aggregates with various morphologies from block copolymers of different compositions (*4*).

Morphological changes can also be induced in an identical block copolymer by the addition of ions in micromolar ($CaCl_2$ or HCl) or millimolar (NaCl) concentrations. The morphologies are the same as those produced by changes in the copolymer composition in the absence of added ions, which suggests that the morphological changes are probably induced by decreased repulsion (both steric and electrostatic) among the hydrophilic segments as a result of protonation of PAA (by HCl) or of ion binding or bridging (by Ca^{2+}). In addition, aggregates of a new morphology, consisting of large compound vesicles (LCVs), were prepared and are described. The LCVs may be useful as possible drug-delivering vehicles and as models of stable microstructured biomaterials. Finally, ion-induced gelation can occur in which spherical micelles in aqueous solution form a cross-linked "pearl necklace" structure in the presence of 20 mM HCl. These results suggest that the versatility of the crew-cut aggregates is much greater than originally suspected.

The PS-*b*-PAA or PS-*b*-PEO diblocks were dissolved in *N*,*N*-dimethylformamide (DMF) to give a stock solution of 1 weight %. Deionized water was then added to the copolymer solutions with stirring; micellization took place between about 4 and 6 weight % of water. However, the addition of water was continued until the solution was 25 weight % of water to ensure that the structure of the formed aggregates was kinetically frozen. We isolated the aggregates into water by dialyzing the resulting solutions against distilled water to remove the DMF. A dynamic equilibrium between aggregates and unimers undoubtedly exists in the early stages of water addition during micellization. At some point, however, as the DMF is forced out of the core, the equilibrium is frozen because of the glassy nature of the PS chains.

Table 1. Summary of the effect of added acid or salt concentration (with *R* given in parentheses) on the aggregate morphology of a PS(410)-*b*-PAA(25) diblock copolymer.

Acid or salt concentration (M) and *R*	Dominant morphology
HCl	
1.9×10^{-4} (0.035)	Spheres
2.1×10^{-4} (0.040)	Rods
2.4×10^{-4} (0.045)	Vesicles
2.7×10^{-4} (0.050)	LCVs
NaCl	
2.1×10^{-3} (0.40)	Spheres
3.2×10^{-3} (0.60)	Rods
1.1×10^{-2} (2.0)	Vesicles
2.1×10^{-2} (4.0)	LCVs
$CaCl_2$	
1.2×10^{-4} (0.023)	Spheres
1.4×10^{-4} (0.026)	Vesicles
2.8×10^{-4} (0.053)	LCVs

Department of Chemistry, McGill University, 801 Sherbrooke Street West, Montreal, Quebec, Canada H3A-2K6.

*To whom correspondence should be addressed.